Spin dynamics in the two-dimensional quantum antiferromagnet La_2CuO_4

K. Yamada,* K. Kakurai, and Y. Endoh*
Department of Physics, Tohoku University, Aramaki, Aoba, Sendai 980, Japan

T. R. Thurston,* M. A. Kastner, and R. J. Birgeneau
Department of Physics, Massachusetts Institute of Technology, Cambridge, Massachusetts 02139

G. Shirane
Brookhaven National Laboratory, Upton, New York 11973

Y. Hidaka and T. Murakami
NTT-Opto-Electronics Laboratories, Nippon Telegraph and Telephone Corporation, Tokai, Ibaraki 319-11, Japan
(Received 10 May 1989)

Using large single crystals (~ 2 cm^3), we have extended previous elastic and inelastic neutron scattering studies of the spin dynamics in the two-dimensional (2D) quantum antiferromagnet La_2CuO_4. We observe well-defined magnetic peaks for constant energy scans across the 2D magnetic rod for a wide range of temperatures and energies. The spectra are compared quantitatively with theoretical models. Simple spin-wave theory satisfactorily describes the experimental results well below T_N. The thermal excitations of the low-energy ($\hbar\omega \leq 3$ meV) spectra, however, appear to deviate from the theory as T_N is approached. The overall temperature and energy dependence of the spectra above T_N (245–520 K) can be explained by the formula of Chakravarty, Halperin, Nelson, and Tyc for the dynamical structure factor $S(\mathbf{q},\omega)$ with no adjustable parameters. We do, however, observe a 2D elastic component which grows rapidly as T_N is approached; it is hypothesized that this arises primarily from magnetic defects and is analogous to the "central peak" observed for many structural phase transitions.

I. INTRODUCTION

Extensive studies of the magnetic properties of $La_{2-x}Sr_xCuO_4$ ($x \leq 0.15$) and $YBa_2Cu_3O_{7-y}$ ($y \leq 1$) (Refs. 1–3) have recently been carried out in order to elucidate the magnetism in these systems and specifically to clarify the potential role of magnetism[4] as a mechanism for the superconductivity. The first neutron scattering experiments[1,2] from La_2CuO_4 revealed a variety of fascinating features including the absence of any appreciable enhancement of the quasielastic component near the Néel temperature (T_N) as well as an enormous energy scale for the spin fluctuations above T_N. These striking properties contrast markedly with the low-energy spin fluctuations in other typical quasi-two-dimensional (2D) antiferromagnets such as K_2NiF_4 (Ref. 5) and K_2CoF_4 (Ref. 6) and those of the isomorphous compounds La_2NiO_4 (Ref. 7) and La_2CoO_4 (Ref. 8) which show dramatic critical-slowing-down phenomena in the 2D spin correlations near T_N. Although the measurements in La_2CuO_4 were done up to 12-meV energy transfer, the spin dynamics seemed to be much akin to the quantum fluctuations in the $S=\frac{1}{2}$ Heisenberg antiferromagnetic linear chain previously observed with neutron inelastic scattering from $CuCl_2 2Py$.[9] Spin excitations in $CuCl_2 2Py$ were observed to form a broad band above the bounded spin-wave mode, $\pi J \sin(qa)$, at $T=0$. Accordingly the highly correlated but fluctuating spin states in La_2CuO_4 were labeled the quantum spin fluid.

These experiments also motivated many theoretical studies to elucidate the basic spin dynamics of the $S=\frac{1}{2}$ 2D Heisenberg antiferromagnet. Chakravarty, Halperin, and Nelson (CHN) (Ref. 10) have analyzed a quantum nonlinear sigma model by combining renormalization-group and dynamic scaling methods and they have proposed formulas for both the static and dynamic structure factors, $S(\mathbf{q}_{2D})$ and $S(\mathbf{q}_{2D},\omega)$, respectively, in the long-wavelength and low-temperature region of the phase diagram. Applying Oguchi's spin-wave theory,[11] they showed that the antiferromagnetic quantum Heisenberg model with $S=\frac{1}{2}$ can be mapped onto the 3D nonlinear sigma model with a coupling constant $g \leq g_c$ which possesses long-range order at $T=0$. Hence, all of the static and dynamic properties can be treated in the classical hydrodynamic limit characterized by the quantum renormalized correlation length (ξ) and the spin-wave velocity (C). More recently, Tyc, Halperin, and Chakravarty have determined the unknown parameters in the CHN model by fitting the CHN formulas to the results of a molecular-dynamical simulation of the classical rotor model.[12] Auerbach and Arovas,[13] using the Schwinger boson mean-field approximation, have obtained similar results without assuming an ordered state at $T=0$. Their calculated results, however, differ from the Tyc, Halperin, and Chakravarty simulations in a variety of subtle ways; we have not attempted to determine experimentally which approach is correct in detail. Rather, because the CHN model is much easier to implement, with a simple

closed-form expression for $S(\mathbf{Q},\omega)$, we shall limit the comparisons of our experimental results to the CHN model alone.

In this study, we have extended the previous neutron scattering measurements on La_2CuO_4. The growth of a very large high-quality single crystal of volume ~ 2 cm^3 has made it possible to expand the experimental range in both temperature and energy and to improve the quality of the data. We have therefore not only carried out inelastic and elastic measurements across the 2D magnetic rod but also have been able to make a critical comparison with the theories. The format of this paper is as follows: In Sec. II we summarize the basic information on La_2CuO_4 relevant to these studies—primarily the crystal and magnetic structures as well as the spin correlations and the spin dynamics. The experimental details are described in Sec. III. The essential predictions of the CHN theory are reviewed in Sec. IV. In Sec. V the 2D magnetic neutron scattering spectra observed by using three-axis (inelastic) and two-axis (elastic) spectrometer modes are presented. These spectra are compared with theory and the overall results are discussed in Sec. VI.

II. PRELIMINARY DETAILS

The crystal and magnetic structures of La_2CuO_4 are shown in Fig. 1. The crystal structure at high temperatures has the same tetragonal symmetry, space group $I4/mmm$, as K_2NiF_4.[5] Below about 500 K, the structure transforms to one with orthorhombic symmetry, space group *Cmca*, due to a staggered tilt of the CuO_6 octahedra as illustrated in Fig. 1. The room-temperature lattice constants are $a=5.354$ Å, $b=13.153$ Å, and $c=5.401$ Å; these correspond to a tilt angle of about 4°. The tilt is uniform in a given *a-b* plane. Since there are two equivalent tilting directions in a CuO_2 basal plane, a twin structure is formed at the structural phase transition.

The Cu^{2+} spins in La_2CuO_4 order antiferromagnetically with a Néel temperature, T_N, of about 240 K and a saturated sublattice moment of about $0.4\mu_B$ for an as-grown crystal. This 3D magnetic order is very sensitive to the oxygen concentration, and specifically as-grown crystals appear to have a slight excess of oxygen. By further oxygenation, the long-range magnetic order decreases at low temperatures with a corresponding increase in 2D short-range order scattering. These effects of the oxygenation on the 3D magnetic properties are similar to those produced by Sr doping in La_2CuO_4.[3] This diminution of 2D order arises from the frustration produced by the spin of the hole on the oxygen atoms between the Cu^{2+} spins.[14] The antisymmetric exchange interaction introduced by the tilt of the octahedra creates a spin canting below T_N in the direction perpendicular to the basal plane as shown in Fig. 1. The canting angle of about 0.2° has been evaluated consistently from both an analysis of the temperature dependence of the uniform magnetic susceptibility near T_N (Ref. 15) and the spin rotation forced by an external magnetic field.[16]

The detailed measurements reported in Ref. 17 reveal that the spin-wave dispersion is isotropic and centered about the antiferromagnetic superlattice position as expected from spin-wave theory for the 2D Heisenberg Hamiltonian. More exotic dynamical structure factors, for example, might be expected from certain versions of the resonating-valence-bond (RVB) model[4] are not found. A lower limit for the 2D spin-wave velocity of about 600 meV Å has been set by constant-E inelastic neutron scattering measurements.[17] The CHN model[10] accounts well for the temperature dependence of ξ determined by the two-axis quasielastic scattering with a spin-wave velocity close to that suggested by the neutron experiment lower limit.[18] Recently Takahashi[19] has obtained a formula for ξ by applying his modified spin-wave theory to the $S=\frac{1}{2}$, 2D Heisenberg antiferromagnet. According to his model the best fit to the previous neutron data determines the spin-wave velocity to be 560 meV Å. Two-magnon Raman scattering measurements, simply interpreted, give the slightly larger value of ~ 740 meV Å.[20]

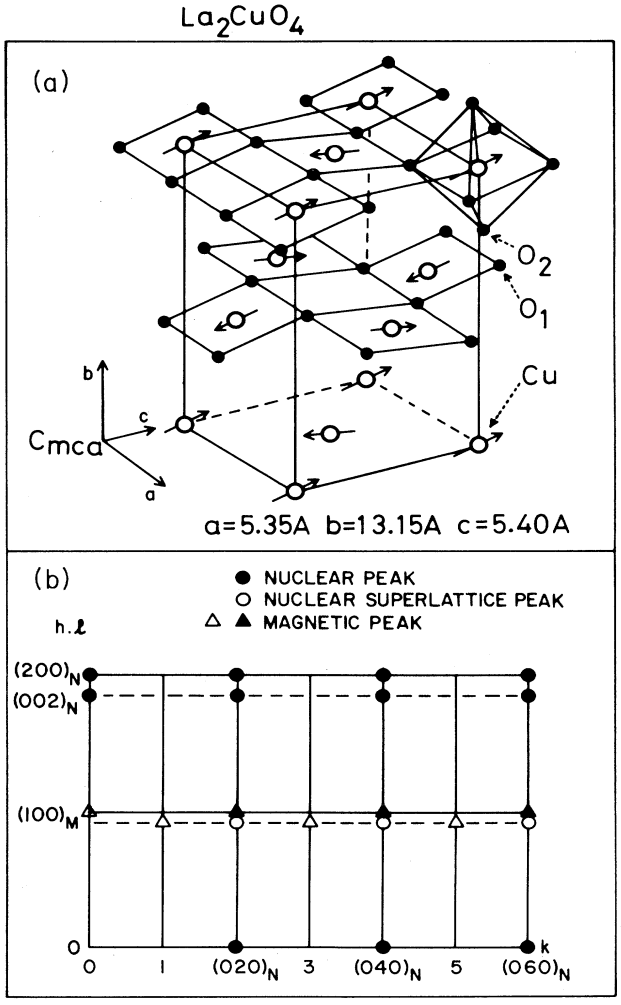

FIG. 1. (a) Spin structure and CuO_2 plane of La_2CuO_4. (b) Reciprocal $a^*(c^*)$-b^* planes supported by the twinned structure in the orthorhombic phase.

Quantum Monte Carlo calculations[21] with this value for the velocity also give good agreement for the experimental ξ's.

According to the previous neutron measurements,[1,2] both the temperature and energy evolution of the constant energy spectrum for $T > T_N$ exhibit significant deviations from those expected from normal spin waves as one might expect. The low-energy, constant-q spectra at low temperatures, however, could be analyzed by normal spin-wave theory to evaluate the anisotropies.[22] These anisotropies generate the energy gaps in the spin-wave dispersion relations: 1.0 ± 0.25 (in-plane mode) and 2.5 ± 0.5 meV (out-of-plane mode). These values are determined by the antisymmetric interaction produced by the tilt and the planar anisotropic exchange, respectively.

III. EXPERIMENTAL DETAILS

Sizable crystals of typical size $20\times20\times5$ mm^3 of La_2CuO_4 were prepared by the CuO flux method.[23] The Néel temperature T_N (=245 K) and the tetragonal-orthorhombic transition temperature T_S (=525 K) were determined from the temperature dependences of the magnetic (1,0,0) and the nuclear superlattice (0,2,1) intensities, respectively (see Fig. 2). The high-temperature measurements up to about 550 K were repeated several times by heating the crystal in vacuum. After the measurements, however, we observed a considerable smearing of the magnetic phase transition; the corresponding change in the structural phase transition was much less, as expected from the order of magnitude difference between dT_N/dO and dT_S/dO where O is the oxygen concentration. Therefore, we used the second crystal for further measurements around T_N. The second crystal (referred to as NTT-8) was cut from the same batch as the first one (referred to as NTT-7) and we confirmed that both crystals exhibited almost identical properties.

The neutron scattering measurements were carried out on the triple-axis spectrometers H4M, H7, H8, and H9 at the Brookhaven High Flux Beam Reactor. Either pyrolytic graphite (0,0,2) or Cu_2MnAl (1,1,1) were used as both monochromator and analyzer for unpolarized or polarized neutron experiments, respectively. Various incident neutron energies together with different horizontal collimations were employed to optimize the different types of measurements. In order to eliminate contamination from higher-order reflections, a cooled beryllium or a pyrolytic graphite filter was inserted in the incident or scattered neutron path. For the low-temperature measurements, the crystal was mounted in an Al can which was charged with 1 atm of He gas as a heat exchanger. The Al can was attached to the cold finger of a liquid-He flow cryostat. The high-temperature measurements were carried out by using a tungsten heater in a furnace pumped down to 10^{-2} torr. The crystal was heated uniformly by radiation from an Al cylinder 100 mm in diameter.

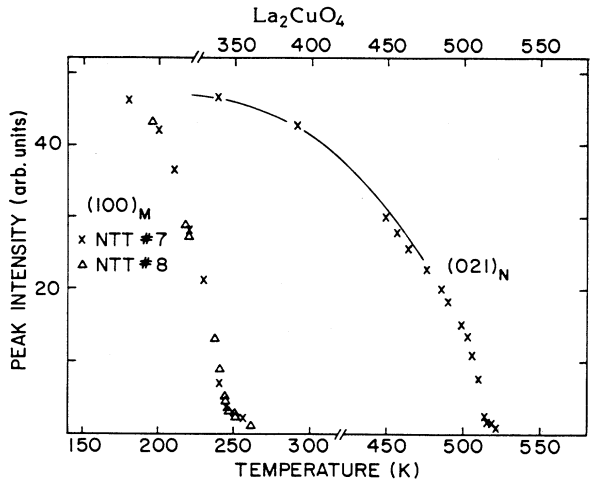

FIG. 2. Temperature dependences of the magnetic (100) and nuclear superlattice (021) Bragg intensities.

The crystal was aligned with an $\mathbf{a}^*$ (and because of the twinning $\mathbf{c}^*$) axis perpendicular to the scattering plane. With this configuration, the 2D magnetic rods were parallel to the scattering plane. In Fig. 1 we show the $\mathbf{a}^*(\mathbf{c}^*)$-$\mathbf{b}^*$ reciprocal plane of the orthorhombic twin structure. In the figure, the open and solid circles denote the nuclear and the superlattice reflections, respectively. The triangles correspond to magnetic reflections; the spin direction for the solid or the open triangles in Fig. 1 is perpendicular or parallel to the scattering plane, respectively.

The static structure factor $S(\mathbf{q}_{2D})$ which describes the instantaneous spin correlations, is given by the following equations:

$$S(\mathbf{q}_{2D})=\int S(\mathbf{q}_{2D},\omega)d\omega \ , \tag{1a}$$

$$S(\mathbf{q}_{2D},\omega)=(2\pi N)^{-1}\int \langle \mathbf{S}(-\mathbf{q}_{2D},0)\cdot\mathbf{S}(\mathbf{q}_{2D},t)\rangle e^{i\omega t}dt \ , \tag{1b}$$

where $\mathbf{q}_{2D}$, the in-plane momentum transfer, is the distance from a magnetic rod in reciprocal space. For 2D magnets, when the outgoing neutron momentum $\mathbf{k}_f$ is parallel to the 2D magnetic rod, an approximate energy integration of Eq. (1a) can be done by a two-axis measurement keeping $\mathbf{q}_{2D}$ constant.[24] Here we call this two-axis scan across the 2D magnetic rod a "focusing scan." Although the integration range is finite, covering approximately the range for $-k_BT$ to the incident neutron energy E_i, the focusing scan has been successfully applied for classical 2D antiferromagnetic systems.[24] ξ could be extracted by fitting the Lorentzian shape function,

$$S(\mathbf{q}_{2D})\propto[(\mathbf{q}_{2D})^2+(1/\xi)^2]^{-1} \ ,$$

to the observed spectra of the two-axis focusing scans convoluted with the instrumental resolution function.

The dynamical structure factor $S(\mathbf{q}_{2D},\omega)$ is measured, in general, by either a constant energy or a constant momentum transfer scan in the three-axis mode as illustrated in Fig. 3. However, because of the very steep dispersion surface of La_2CuO_4, as well as the finite E and q experimental resolution, it was difficult to obtain proper information on the integrated intensity for the spectrum of $S(\mathbf{q}_{2D},\omega)$ from constant-q scans. Therefore, we per-

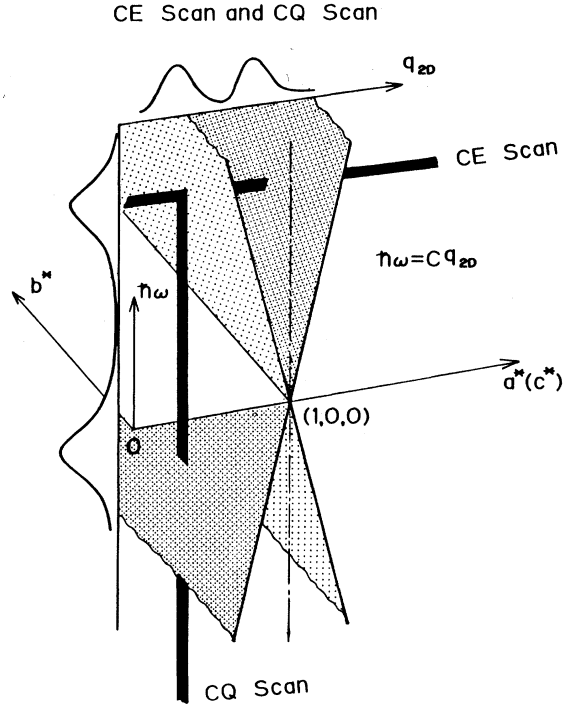

FIG. 3. Constant energy (CE) and constant momentum (CQ) scans in the schematic 2D dispersion surface.

formed exclusively constant-E scans. For the same reason, however, the constant-E scan across a magnetic rod could not resolve the $\pm\mathbf{q}_{2D}$ contributions from the symmetric dispersion surface. Most of the three-axis measurements were carried out varying the incident neutron energy while keeping the final energy constant (constant-E_f mode). In this mode, the monitor value for the incident neutron flux must be corrected for the energy-dependent higher-order contamination. For a typical energy transfer of 6 meV, the energy resolution was ~ 1.4 meV full width at half maximum (FWHM) while the momentum resolution projected onto the **a*-b*** plane was 0.12 Å^{-1} FWHM.

IV. REVIEW OF RELEVANT THEORY

Here we follow the discussion given in Refs. 10 and 12; the argument by CHN is that the $S(\mathbf{q}_{2D},\omega)$ of the 2D quantum Heisenberg antiferromagnet may be directly related to that of a classical lattice rotor model which can be studied by molecular-dynamics simulations. This argument may apply for the spin dynamics only at sufficiently low temperatures and energies and close to the magnetic rod.

According to CHN, the correlation length ξ derived from the two-loop renormalization-group analysis can be transformed into the following formula for the quantum Heisenberg antiferromagnet:

$$\xi^{-1}=\kappa=\frac{(1+T/2\pi\rho_s)}{Da}\exp(-2\pi\rho_s/T)\ , \tag{2}$$

$$2\pi\rho_s\sim 0.576(hC/a)\ , \tag{3}$$

where D is a constant which is about 0.5, ρ_s is the spin stiffness at $T=0$, C is the spin-wave velocity, and a is the lattice constant in the tetragonal basal plane (3.79 Å).

In the scaling regime, the dynamical structure factor can be written in the form

$$S(\mathbf{q}_{2D},\omega)=\omega_0^{-1}S(\mathbf{q}_{2D})\phi(k,\nu) \tag{4}$$

with the characteristic frequency

$$\omega_0=C\xi^{-1}(T/2\pi\rho_s)^{1/2}\ . \tag{5}$$

The scaling variables are defined as $\nu=\omega/\omega_0$ and $k=q_{2D}\xi$. According to the renormalization-group analysis, $S(\mathbf{q}_{2D})$ has the scaling form

$$S(\mathbf{q}_{2D})=S(\mathbf{q}_{2D}=0)f(k)\ , \tag{6}$$

$$f(k)\approx[1+0.5B_f\ln(1+k^2)]/(1+k^2)\ , \tag{7}$$

$$S(\mathbf{q}_{2D}=0)=Bs\xi^2N_0^2/[(2\pi\rho_s/T)+1]^2\ . \tag{8}$$

According to Ref. 12, their molecular-dynamics results were fit with a two-Lorentzian form for the dynamical scaling function,

$$\phi(k,\nu)\approx\gamma_k\{[(\nu-\nu_k)^2+\gamma_k^2]^{-1}+[(\nu+\nu_k)^2+\gamma_k^2]^{-1}\}\ . \tag{9}$$

The formulas for the dimensionless spin-wave frequency ν_k and the width γ_k include four adjustable parameters: γ_0, μ, θ, and δ,

$$\nu_k\approx(\tfrac{3}{2})^{1/2}k[\delta+0.5\ln(1+k^2)]^{1/2}\ , \tag{10}$$

$$\gamma_k=\gamma_0(1+\mu k^2)^{1/2}[1+(\theta/2)\ln(1+k^2)]^{-3/2}\ . \tag{11}$$

The details of these expressions and the simulation method are described in Ref. 12. Here we simply summarize the parameters obtained by fitting these expressions to the dynamical simulation of the classical linear rotator model. Tyc, Halperin, and Chakravarty[12] determined these parameters as the following: $B_f=0.10$, $B_S=125$, $\delta=1.05$, $\gamma_0=0.86$, $\mu=1.4$, and $\theta=0.08$. Accordingly, in order to compare this model with experiment we need as adjustable parameters only the spin-wave velocity C which, within the context of this theory, will be determined by the measured static correlation lengths, $\xi(T)$, and an overall intensity scale factor. Finally, for comparison with experiment we multiply Eq. (4) by the additional factor $\omega(1-e^{-\hbar\omega/k_BT})^{-1}$ to make the connection between classical and quantum statistics and explicitly to ensure that detailed balance is satisfied.

V. EXPERIMENTAL RESULTS

A. Basic character of the 2D spin correlations

In this section we present measurements of the basic features of the 2D spin correlations for the present crystals. As shown in Fig. 4, three-axis spectra across the magnetic rod $(1,K,0)$ [or $(0,K,1)$] at different K are al-

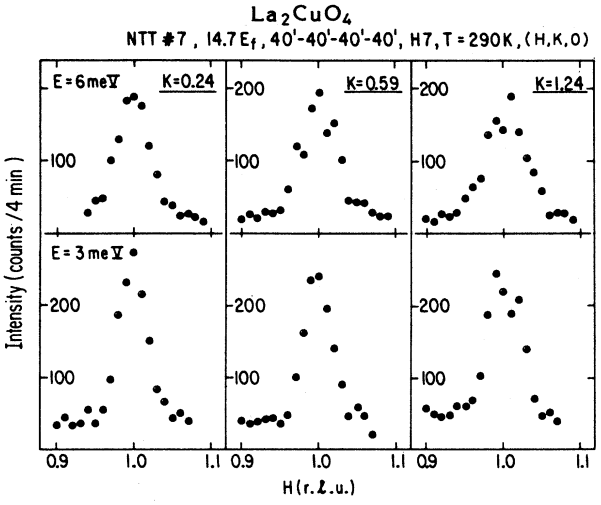

FIG. 4. Three-axis constant-E_f scans across the magnetic rod $(1,K,0)$ [or $(0,K,1)$] at different K values above T_N.

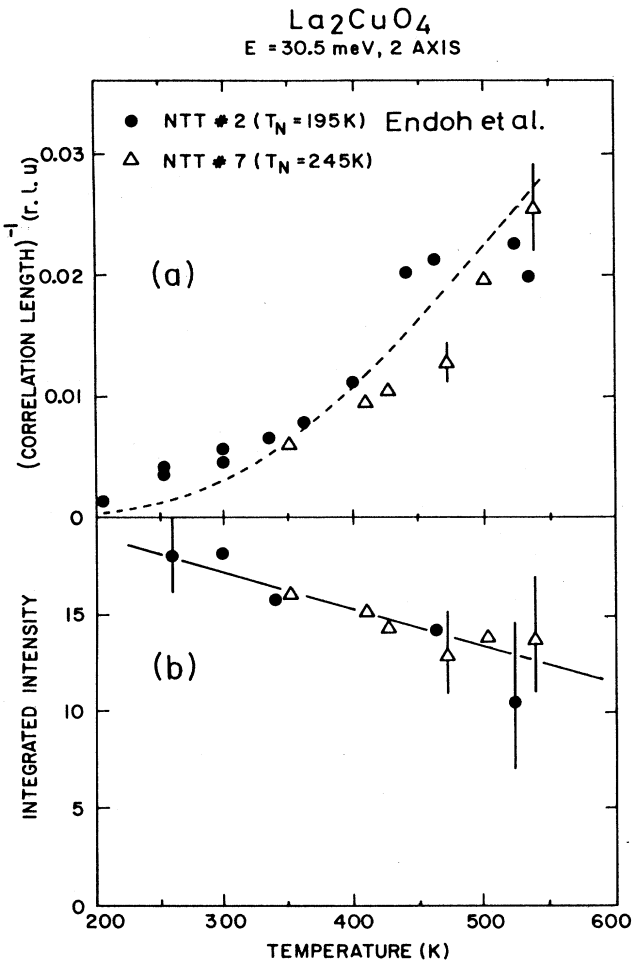

FIG. 5. Temperature dependences of (a) inverse correlation length κ and (b) integrated intensity measured by two-axis focusing scan.

most identical within the experimental accuracy. Therefore, we reconfirm the two dimensionality of the dynamical response function $S(\mathbf{q}_{2D},\omega)$ of this system; this is an essential requirement for the following discussion. It should be noted that the magnetic form factor $f(\mathbf{Q})$ is almost constant[25] within the K range probed in Fig. 4. We have also observed the third-order 2D rod $(3,K,0)$ [or $(0,K,3)$] whose intensity indeed follows the magnetic form factor[25] as expected. In addition, we confirmed that the 2D inelastic response is magnetic in origin by using polarized neutron techniques.

The temperature dependence of ξ in the 2D plane has been studied utilizing the two-axis focusing scans as in Ref. 2. An incident neutron energy of 30.5 meV was utilized; this should integrate over the important low-energy spin fluctuations. The inverse correlation length κ as a function of the temperature so obtained is plotted in Fig. 5 together with the previous results obtained from a crystal with $T_N=195$ K. The two sets of measurements agree well in spite of the difference in T_N for the two crystals. Indeed, the shifts in the average ξ are consistent with the differences in T_N for the two crystals. The dotted line in Fig. 5 is calculated using Eq. (2) with the spin-wave velocity $C=850$ meV Å. Clearly the CHN model accounts quite well for the static structure factor. The inferred spin-wave velocity is somewhat higher than that suggested by earlier measurements but agrees well with the results of recent epithermal neutron scattering experiments by Aeppli and co-workers.[26]

B. The dynamical structure factor

We first discuss the results of the three-axis inelastic scans (constant E_f) across the magnetic rod $(1,K,0)$ [or $(0,K,1)$] in the 3D long-range ordered state below T_N. Typical spectra at three temperatures are presented in Fig. 6. The temperature evolution of these spectra seems to follow reasonably Bose statistics as expected for har-

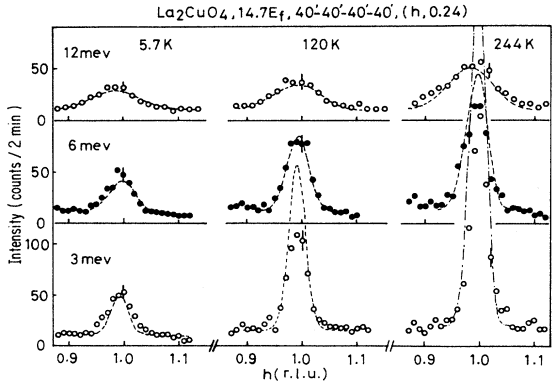

FIG. 6. Temperature evolutions of constant energy scans across the magnetic rod below T_N. The effects of the energy dependence of the higher-order reflection on the incident neutron monitor have been corrected for. The dashed lines in the figure are calculations from a normal spin-wave formula convoluted with the instrumental resolution function (see the text).

monic spin waves and as observed previously.[2] To examine the applicability of ordinary spin-wave theory more critically we have performed a detailed comparison between our experiment results and the predictions of spin-wave theory for $S(\mathbf{q}_{2D},\omega)$ including the energy gaps,

$$S^{SW}(\mathbf{q}_{2D},\omega)\sim\gamma\omega_p^{-1}\{[(\omega-\omega_p)^2+\gamma^2]^{-1}[n(\omega)+1] +[(\omega+\omega_p)^2+\gamma^2]^{-1}n(\omega)\}\ . \quad (12)$$

In the above equation, the dispersion relation and the Bose occupation factor are as follows: $\omega_p^2=(Cq_{2D})^2+E_g^2$ and $n(\omega)=(e^{\hbar\omega/k_BT}-1)^{-1}$, where E_g is the energy gap due to the anisotropy; $E_g=1.0\pm0.25$ meV for the in-plane mode and 2.5 ± 0.05 meV for the out-of-plane mode have been determined by an independent neutron study on La_2CuO_4.[22] We initially took as the spin-wave velocity $C=650$ meV Å and the linewidth γ was fixed at 1 meV. The overall intensity scale factor was obtained by fitting the calculation to the spectrum at 6 meV for $T=120$ K. The temperature dependences of the gap energies were included explicitly in the calculations. The relative intensity and the shape of the calculated spectra were found to be insensitive for the range of input values $C=650-850$ meV and $\gamma\leq1$ meV. This happens presumably because the measured spectra are all resolution limited. As is evident in Fig. 6, the calculations agree fairly well with experiment at low temperatures $T\leq120$ K. As the temperature is increased up to T_N, however, the deviation between the two grows, especially for the 3-meV excitation spectrum.

In Fig. 7 we show the temperature evolution of the same set of scans as in Fig. 6 but *above* T_N. This temperature evolution cannot be explained by normal spin-wave theory as was pointed out in our previous study.[1,2] Accordingly we instead make a detailed comparison with the predictions of the CHN model as presented in Sec. IV. The results are shown by the dashed lines in Fig. 7. In these calculations we use $C=850$ meV Å as determined by the static correlations and the ξ's were fixed at their measured values so that there is only one remaining adjustable parameter—the overall intensity scale. This scale factor was fixed by matching the theory to experiment for the $E=6$-meV spectrum at 290 K. Thus, all of the remaining spectra are calculated without any adjustable parameters. Clearly the agreement between the CHN model and experiment is excellent. It is especially notable that the theory was carried out in advance of and entirely independent of our experiments.

A corresponding set of scans for $E=0$ is shown in Fig. 8. The $E=0$ intensity clearly grows dramatically as the temperature is decreased. As we shall discuss below, this behavior is not predicted by the CHN model. We summarize the temperature dependences of the integrated intensities at different energies both below and above T_N in Fig. 9. The intensities of the low-energy excitations show a peak around T_N. Most notably, the elastic intensity seems to be diverging near T_N. On the other hand, the higher-energy spectra depend only weakly on the temperature. The data taken at different K are combined in the figure. We will discuss these intensities in more detail in the next section.

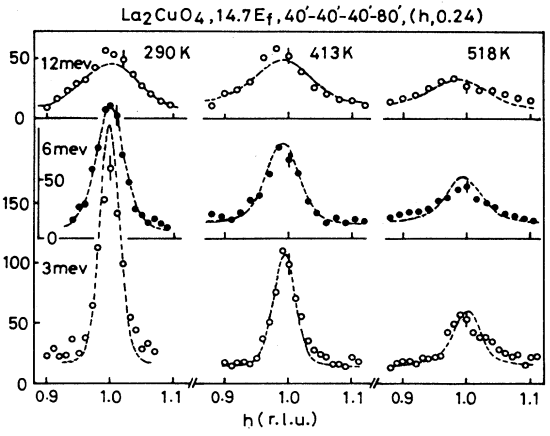

FIG. 7. Temperature evolution of constant energy scans across the magnetic rod above T_N. The effects of the energy dependence of the higher-order reflection on the incident neutron monitor have been corrected for. The dashed lines in the figure are the results of calculations utilizing the CHN formula for the dynamical structure factor convoluted with the experimental resolution function (see the text).

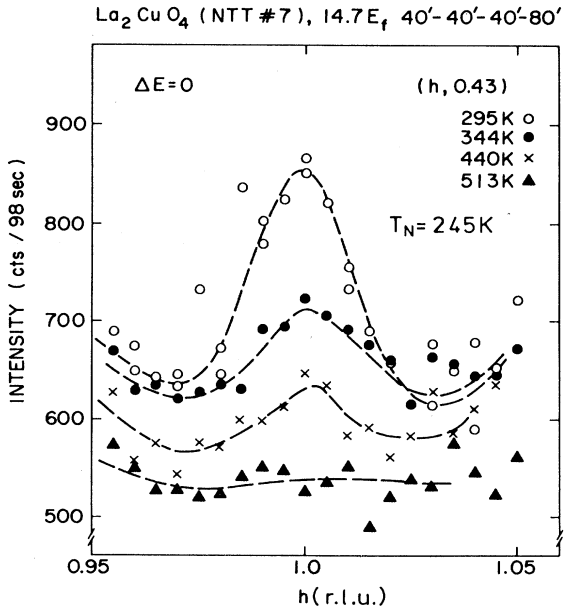

FIG. 8. Temperature evolution of elastic scans across the magnetic rod. The lines are guides to the eye.

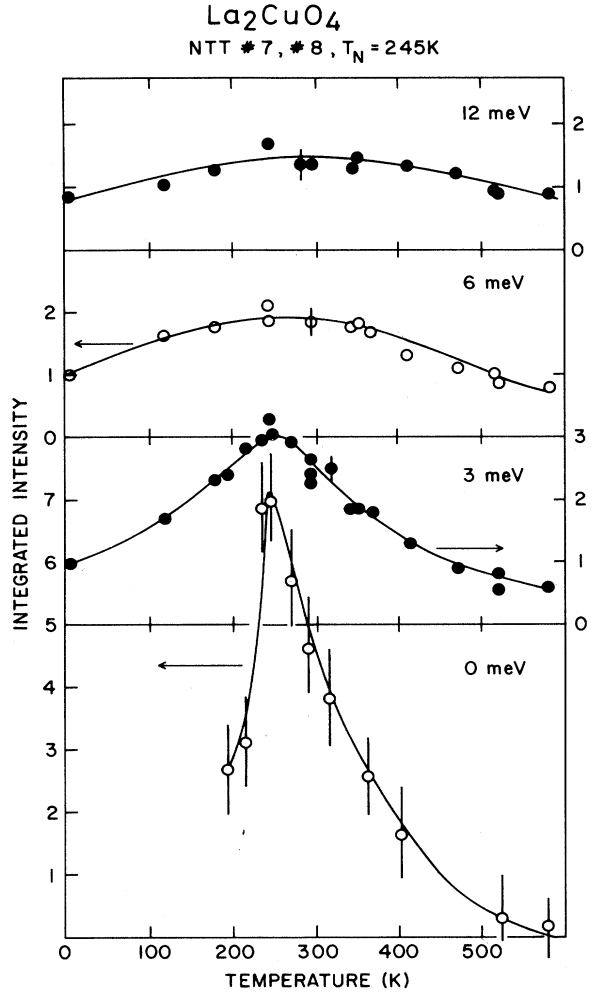

FIG. 9. Temperature dependences of the integrated intensities of constant energy scans across the magnetic rod at different energies. The lines are guides to the eye.

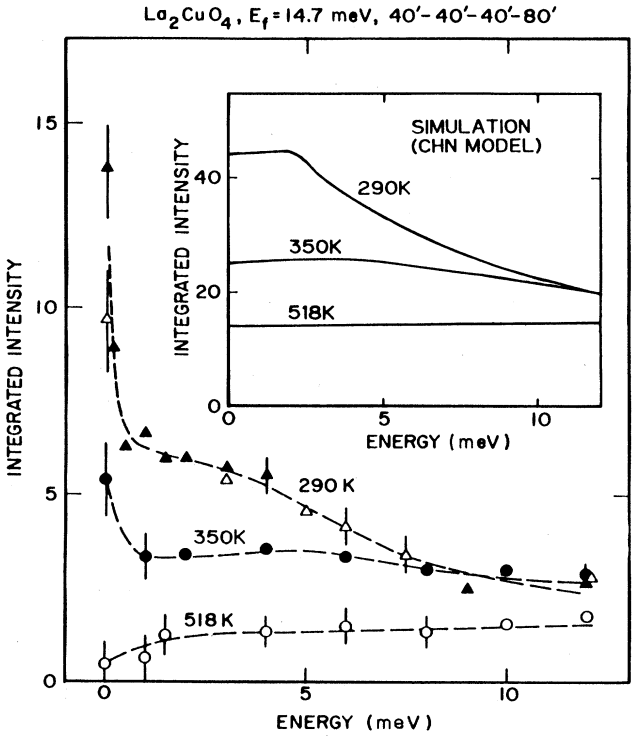

FIG. 10. Energy dependences of integrated intensities of constant energy scans across the magnetic rod at different temperatures. The data at 290 K are taken from two crystals NTT-7 (open triangle) and NTT-8 (solid triangle). The inset is the results of calculations utilizing the CHN model (see the text).

VI. DISCUSSION

We begin with a discussion of $S(\mathbf{q}_{2D},\omega)$ of La_2CuO_4 for $T \leq T_N$; that is, in the Néel state. Satisfactory agreement is obtained between the predictions of normal spin-wave theory and the experimental spectra at low temperatures as shown in Fig. 6. As the temperature is increased the calculation deviates somewhat from the experiment at least at the lowest energy. This presumably reflects the effects of magnon-magnon interactions which are not included in the calculations. At higher energies, especially at 12 meV, the agreement is quite satisfactory.

We now discuss $S(\mathbf{q}_{2D},\omega)$ above T_N. In Fig. 10 we plot the integrated intensities of the constant energy scans as a function of energy above T_N. The inset in Fig. 10 is the prediction of the CHN model including resolution effects. The overall agreement between the calculation and the experiment is quite good except in the quasielastic regime. The most unusual feature of the predicted energy dependence is that a characteristic broad peak or plateau at $E \neq 0$ appears in the simulation; this is in contrast to conventional theory which gives a Lorentzian form centered at $E=0$. This peak shifts to higher energies and smears as the temperature increases. The experimental results are consistent with this picture. It should be noted that the integrated intensity expected from the CHN model without the resolution effects decreases monotonically as the energy increases although the intensity at $\omega=0$ is largely suppressed compared with normal Lorentzian dynamical structure. To elucidate the reason for this unusual energy dependence, we further simulated the constant energy scans using the normal spin-wave formulas as well as the normal paramagnetic scattering cross section.[27] The integrated intensities utilizing both formulas were found to exhibit monotonic energy dependences with peaks centered at $E=0$. Therefore, we speculate that the unusual spectra shown in Fig. 10 reflect both effects; that is, resolution effect and a characteristic form of $S(\mathbf{q}_{2D},\omega)$ which describes a spin wave with a finite correlation length. It should be emphasized, as just mentioned above, that the scattering function with both a finite correlation length and a spin-wave dispersion relation suppresses the intensity at $q=0$ and $\omega=0$. This reflects the crossover behavior from the overdamped to the propagating regime combined with the resolution

effects. So far such a crossover has been directly observed by constant-q scans only in the 1D case,[28] where the critical regime is rather large even for classical spins due to the one dimensionality. The characteristic energy dependence shown in Fig. 10, therefore, is considered to be evidence for the existence of the dispersion surface as illustrated in Fig. 3. It should be noted that the plateau or peak at $E \neq 0$ in Fig. 10 differs quantitatively from the peak observed in constant energy scans of paramagnetic scattering in the critical regime.[27] The temperature dependence of the integrated intensities is shown in Fig. 11; again, there is excellent agreement between experiment and the CHN theory except in the elastic region. The lines in the figure represent a smooth interpolation between the results of the calculations at four temperatures 290, 365, 413, and 518 K.

The 2D elastic component grows with decreasing temperature more rapidly than the inelastic components as shown in Figs. 9 and 11. Since this temperature dependence seems to be related to the incipient 3D magnetic order, we performed high-resolution measurements near T_N. The temperature evolution of the 2D component is found to be much less divergent than that of the 3D order as shown in Fig. 12. Therefore this component is not diverging toward T_N but rather probably toward $T=0$. However, once long-range order is established, the elastic component of the magnetic rod begins to concentrate onto the Bragg peaks thence causing a drastic drop of the 2D intensity below T_N (see Fig. 9). We speculate that this $E=0$ component arises primarily from magnetic defects and that it corresponds to a "central peak" by analogy with the central peak commonly observed at structural phase transitions.[29] Further measurements are required to test this idea.

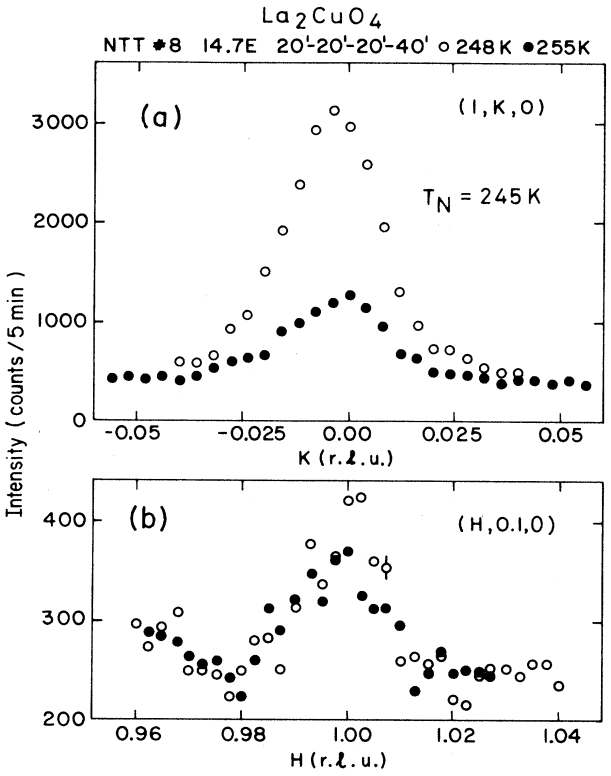

FIG. 12. Elastic spectra measured (a) around the (1,0,0) Bragg point, and (b) around the magnetic rod just above T_N.

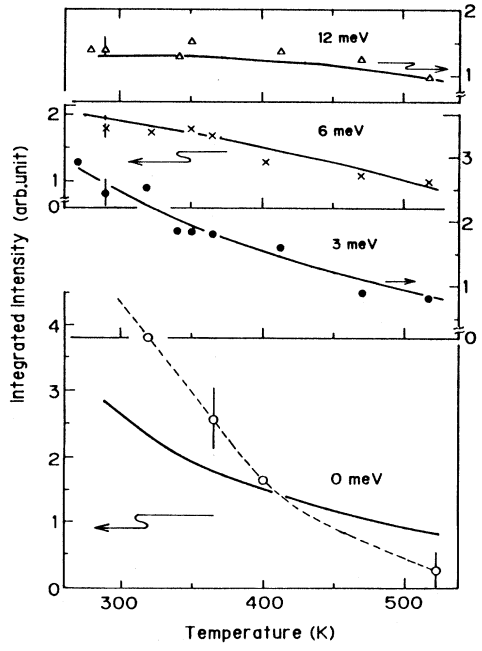

FIG. 11. Temperature dependences of the integrated intensities of constant energy scans across the magnetic rod at different energies. The solid lines are the results of calculations utilizing the CHN model.

As emphasized in Ref. 2, La_2CuO_4 does not show the dramatic critical slowing down behavior exhibited by other planar antiferromagnets such as K_2NiF_4 (Ref. 5) and La_2NiO_4.[7] The reason for this difference is now clear. In the latter materials, the Néel transition is driven by the crystal-field anisotropy so that the critical behavior is that of the 2D Ising model. In that case the characteristic frequency scales like ξ^{-2}. However, in La_2CuO_4 the anisotropy plays a minor role and, as is evident from Eq. (5), one expects $\omega_0 \sim \xi^{-1}$. In the well-correlated regime when $\xi/a \sim 100$ this will produce a factor of ~ 100 difference in the characteristic energies.

In conclusion, our detailed quasielastic and inelastic neutron scattering results show that the main features of the spin fluctuations in La_2CuO_4 above T_N can be well understood within the quantum renormalized classical spin model and indeed the overall agreement with the CHN prediction is quite good. The deviation from the Bose statistics observed above T_N in the previous measurement[2] turns out to be a manifestation of the greatly overdamped nature of the low-energy excitations. Below T_N, satisfactory agreement with normal spin-wave theory is obtained except near T_N.

ACKNOWLEDGMENTS

We thank S. Chakravarty for sending us a copy of Ref. 12 prior to publication. We are grateful for stimulating discussions with A. Auerbach, B. I. Halperin, G. Reiter, J. Tranquada, and M. Takahashi. Two of the authors (K.Y. and Y.E.) also are thankful for the hospitality of the members of the neutron scattering group in the Brookhaven National Laboratory. This work was supported by U.S.-Japan Cooperative Neutron Scattering Program. The work at Tohoku University was supported by the Grant in Aid for the Scientific Research Project. The research at Brookhaven is supported by the division of Materials Science, U.S. Department of Energy under Contract No. DE-AC02-76CH00016. The work at MIT was supported by the National Science Foundation under Contract Nos. DMR85-01856, DMR84-18718, and DMR87-19217.

---

*Visiting scientist at Brookhaven National Laboratory.

[1]G. Shirane, Y. Endoh, R. J. Birgeneau, M. A. Kastner, Y. Hidaka, M. Oda, Y. Enomoto, M. Suzuki, and T. Murakami, Phys. Rev. Lett. **59**, 1613 (1987).

[2]Y. Endoh, K. Yamada, R.J. Birgeneau, D. R. Gabbe, H. P. Jenssen, M. A. Kastner, C. J. Peters, P. J. Picone, T. R. Thurston, J. Tranquada, G. Shirane, Y. Hidaka, M. Oda, Y. Enomoto, M. Suzuki, and T. Murakami, Phys. Rev. B **37**, 7443 (1988).

[3]R. J. Birgeneau and G. Shirane, in *Physical Properties of High Temperature Superconductors,* edited by D. M. Ginsberg (World-Scientific, Singapore, 1989), and references therein.

[4]P. W. Anderson, Science **235**, 1196 (1987).

[5]R. J. Birgeneau, H. J. Guggenheim, and G. Shirane, Phys. Rev. B **1**, 2211 (1970).

[6]H. Ikeda, J. Phys. Soc. Jpn. **37**, 660 (1974).

[7]G. Aeppli and D. J. Buttrey, Phys. Rev. Lett. **61**, 203 (1988).

[8]K. Yamada, M. Matsuda, Y. Endoh, B. Keimer, R. J. Birgeneau, S. Onodera, J. Mizusaki, T. Matsuura, and G. Shirane, Phys. Rev. B **39**, 2336 (1989).

[9]Y. Endoh, G. Shirane, R. J. Birgeneau, P. M. Richards, and S. L. Holt, Phys. Rev. Lett. **26**, 18 (1974).

[10]S. Chakravarty, B. I. Halperin, and D. R. Nelson, Phys. Rev. B **39**, 2344 (1989).

[11]T. Oguchi, Phys. Rev. **117**, 117 (1960).

[12]S. Tyc, B. I. Halperin, and S. Chakravarty, Phys. Rev. Lett. **62**, 835 (1989).

[13]D. P. Arovas and A. Auerbach, Phys. Rev. Lett. **61**, 617 (1988); Phys. Rev. B **38**, 316 (1988).

[14]Amnon Aharony *et al.*, Phys. Rev. Lett. **60**, 1330 (1988).

[15]Tineke Thio, T. R. Thurston, N. W. Preyer, P. J. Picone, M. A. Kastner, H. P. Jenssen, D. R. Gabbe, C. Y. Chen, R. J. Birgeneau, and Amnon Aharony, Phys. Rev. B **38**, 905 (1988).

[16]M. A. Kastner, R. J. Birgeneau, T. R. Thurston, P. J. Picone, H. P. Jenssen, D. R. Gabbe, M. Sato, K. Fukuda, S. Shamoto, Y. Endoh, K. Yamada, and G. Shirane, Phys. Rev. B **38**, 6636 (1988).

[17]R. J. Birgeneau *et al.*, Phys. Rev. B **38**, 6614 (1988).

[18]P. W. Anderson, Science **235**, 1196 (1987).

[19]M. Takahashi, Phys. Rev. B **40**, 2494 (1989).

[20]K. B. Lyons *et al.*, Phys. Rev. B **37**, 2353 (1988).

[21]G. Gomez-Santos, J. D. Joannopoulos, and J. W. Negele, Phys. Rev. B **39**, 4435 (1989).

[22]C. Peters *et al.*, Phys. Rev. B **37**, 9761 (1988).

[23]Y. Hidaka *et al.*, J. Cryst. Growth **85**, 581 (1987).

[24]R. J. Birgeneau, J. Als-Nielsen, and G. Shirane, Phys. Rev. B **16**, 280 (1977).

[25]T. Freltoft, G. Shirane, S. Mitsuda, J. P. Remeika, and A. S. Cooper, Phys. Rev. B **37**, 137 (1988).

[26]G. Aeppli, S. M. Hayden, H. A. Mook, Z. Fisk, S.-W. Cheong, D. Rytz, J. P. Remieka, G. P. Espinosa, and A. S. Cooper, Phys. Rev. Lett. **62**, 2052 (1989).

[27]Y. J. Uemura *et al.*, Phys. Rev. Lett. **51**, 2322 (1983).

[28]J. K. Kjems *et al.*, J. Magn. Mater. **31-34**, 1133 (1983).

[29]See for example, S. M. Shapiro, J. D. Axe, G. Shirane, and T. Riste, Phys. Rev. B **6**, 4332 (1972).